ARTICLE

Exploring the tunable optical and mechanical properties of multicomponent low molecular weight gelators

Received 00th January 20xx,
Accepted 00th January 20xx

DOI: 10.1039/x0xx00000x

Jeanette N. Loos[a], Charlotte E. Boott[a], Dominic W. Hayward[b], Gabriel Hum[c] and Mark J. MacLachlan[ade]

A class of amino acid-based low molecular weight gelators (LMWGs) was used for single and multicomponent gel studies to investigate their tunable optical properties and their self-assembly process. The optical properties of multicomponent gels were found to be easily tuned by changing the proportion of the components, varying from opaque to highly transparent gels as analyzed using UV-vis spectroscopy. This unique phenomenon allows tunability without introducing another variable into the system. Scanning electron microscopy (SEM), differential scanning calorimetry (DSC) and small angle X-ray scattering (SAXS) were used to investigate the underlying self-assembly processes that give rise to observed tunability. It was found that, due to the structural similarities of the molecules, the gelators favor co-assembly packing over self-sorting. The emergence of transparency was ascribed to changes in the fibre diameters. Moreover, analysis of the SAXS data allowed us to compare the molecular order present in the gel phase with single crystal X-ray diffraction (SCXRD) data. Our analysis suggests that the packing of molecules seen in a crystal is translated into the gel network. This reveals that the structure of the crystalline phase seen through SCXRD is a useful tool to aid in understanding the molecular packing in the gel phase.

Introduction

Gels are three-dimensional (3D) soft solids that are widely used in applications ranging from biomedicine[1–3] to electronics[4–6]. They have an interconnected 3D network that can retain a high volume of solvent (>90% in some cases). A gel can be classified as either a hydrogel or organogel depending on the adsorbent (water or organic solvent, respectively) and either a chemical or physical gel based on the interactions that hold the network together. Chemical gels usually contain covalently crosslinked networks; the most common examples are polymeric gels, where polymer chains are entangled to form the interconnected network[2]. These gels are used in contact lenses and drug delivery systems[1–3]. Physical gels, such as molecular or colloidal gels, form networks through non-covalent interactions including hydrogen bonding, ionic bonding, and hydrophobic interactions[7], and are of great interest for uses in cell culturing, optoelectronics, sensing and catalysis[8,9,18–20,10–17].

Supramolecular gels are a sub-class of physical gels, and they are often prepared from low molecular weight gelators (LMWGs). In these systems, a gel arises when the LMWGs self-assemble into extended structures, such as fibres or ribbons, through non-covalent interactions. At sufficiently high concentrations, these fibres intertwine into a 3D network that can immobilize the solvent (Figure 1). Due to the weak nature of non-covalent interactions, the gels respond to external stimuli, such as heat, which disrupts the crosslinking through energy input[21]. The reversible assembly of supramolecular gels suggests they can be produced and moulded easily from a solution containing the gelator, forming an entangled network and, thus, a gel with the correct stimulus. Gel formation can be triggered when the gelator is dissolved in a hot solvent and the solution is cooled, concentration is increased, or through the

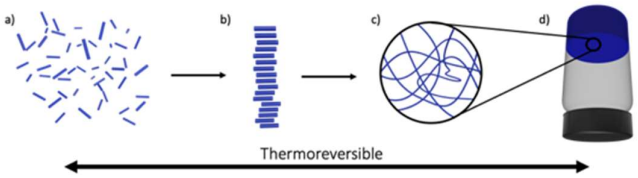

Fig. 1 Schematic representation of the thermoreversible assembly of a low molecular weight gelator (LMWG) into a bulk gel. a) LMWG dispersed in solution. b) LMWG self-assembles upon addition of a trigger (e.g. heat) into fibrillar structures. c) Gel network formed through entanglement of fibres. d) Self-supporting gel that can immobilize solvent.

[a] *University of British Columbia, Department of Chemistry, 2063 Main Mall, Vancouver, British Columbia V6T 1Z1, Canada.*
[b] *Jülich Centre for Neutron Science, Forschungszentrum Jülich GmbH, Outstation at MLZ, Lichtenbergstraße 1, 85747 Garching, Germany.*
[c] *BC Research Inc., 12920 Mitchell Road, Richmond, British Columbia V6V 1M8, Canada.*
[d] *Stewart Blusson Quantum Matter Institute, 2355 East Mall, Vancouver, British Columbia V6T 1Z4, Canada.*
[e] *WPI Nano Life Science Institute, Kanazawa University, Kanazawa, 920-1192, Japan.*

† Footnotes relating to the title and/or authors should appear here.
Electronic Supplementary Information (ESI) available. CCDC 2021380. For ESI and crystallographic data in CIF format, see DOI: 10.1039/x0xx00000x

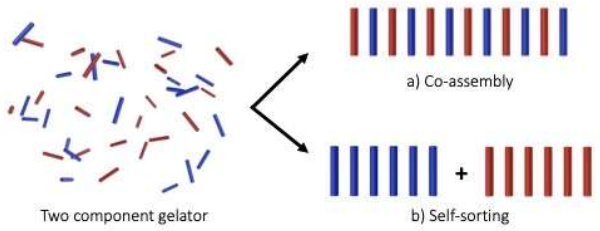

Fig. 2 Schematic representation of a two gelator component system where both compounds can themselves form a gel. a) Both gelators interact with each other leading to co-assembly. b) Each gelator only interacts with its own type, leading to self-sorting.

addition of a poor solvent that can initiate the self-assembly required for gelation[7].

Gelation occurs when molecules have the correct features and properties within the system to create an interconnected network to immobilize the solvent. The LMWG molecules need to have an appropriate solubility in the desired solvent to avoid remaining in solution or precipitating. This balance is crucial for gelation and can easily be tuned through control of the substituents (often alkyl chains) on the LMWG. The substituents can be modified to assist in the gelation process through van der Waals forces, strengthening the interactions between molecules within a gel system. Furthermore, the molecular design should include features to form non-covalent interactions, such as hydrogen bonding, for self-assembly to occur; these components are usually positioned in the head group of the molecule[22].

Supramolecular gels can be formed by single-component LMWGs, or from multicomponent gelator systems. Buerkle and Rowan[7] have defined three main types of multicomponent gel systems: (1) a two component gel-phase where both compounds are necessary to form a gel; (2) a two component gelator where both compounds themselves form a gel; and (3) a system containing a gelator and a non-gelating additive. System 2 can be further classified as either co-assembled or self-sorting, based on the interactions of the LMWG when forming the fibrillar network. In co-assembly, the two LMWGs interact with each other as they assemble, whereas in self-sorting each LMWG prefers to assemble with itself (Figure 2).

We recently reported a study on the effect of substituting a carboxylic acid with a primary amide on the gelation behaviour of several amino acid-based LMWGs[23]. In that report, we found that the use of a primary amide instead of the carboxylic acid reduced the minimum gelling concentration (MGC) across a range of solvents and improved the thermal and mechanical properties of the gel. Herein, we took the best three primary amide LMWGs (i.e. those with the lowest minimum gelling concentrations) from this class of molecules and investigated the impact of mixing two LMWGs on the resulting gels. It was found that the optical properties of the mixed gel system could be tuned from opaque to highly transparent gels by changing the mass ratio of the LMWGs. The study of mixed component gel systems in varying ratios to tune gels from transparent to opaque has not been widely explored. The gels were characterized using UV-vis spectroscopy, rheology, scanning electron microscopy (SEM), differential scanning calorimetry (DSC) and X-ray scattering to gain insight into how the LMWG self-assembly occurs in order to understand the mechanical and optical properties of the LMWG mixtures. Although single-component supramolecular gels have been extensively studied, multicomponent systems are more complex and difficult to study since the effects of introducing an additional component are still unpredictable[24]. The aim of this research is to broaden current knowledge in determining the link between the bulk properties of a gel and its internal structure. Going forward, this structure-property relationship can be employed to produce new gel formulations with fine control over the bulk properties.

Materials and methods

All reagents were commercially available and used as received unless otherwise noted. Decane, chloroform, triethylamine and lauroyl chloride were purchased from Sigma-Aldrich. Amino acid amides were purchased from Oakwood Chemical. ^{1}H NMR spectra were recorded on a Bruker Avance 400inv NMR spectrometer. Mass spectrometry was run on a Waters ZQ equipped with an ESCI ion source at the UBC Chemistry Mass Spectrometry Centre.

Synthesis and gel preparation

LMWGs **1**-**3** (Figure 3b), were prepared using a similar procedure as previously reported[23]. For example, triethylamine (1.39 g, 2.2 molar equivalent) was added in one aliquot to a cooled (0 °C) solution of the L-valinamide hydrochloride (1.0 g, 1.0 molar equivalent) dissolved in chloroform (50 mL). Lauroyl chloride (1.58 g, 1.1 molar equivalent) was added dropwise at 0 °C and the reaction was stirred overnight at room temperature. The desired product was isolated by suction filtration, washed with chloroform and water, then purified by recrystallization in pure methanol. The same procedure was repeated with L-alaninamide hydrochloride and L-phenylalaninamide to produce compounds **1**-**3** (**1** = 64%, **2** = 74%, **3** = 81% yields). The gels were prepared in decane at concentrations ranging from 2 to 10 mg/mL by heating the sample with a heat gun (~120 °C) until a clear, homogenous solution was observed and then left to cool down to room temperature under ambient conditions. The mixed gel systems were prepared using the same method, but with varying mass ratios of the LMWGs.

Minimum gelling concentrations

Minimum gelling concentrations (MGCs) were obtained as weight percent (wt%) and determined by using the inversion test[25]. In a test, the gelators (e.g. one or two LMWGs up to a total of 5 mg) were added to a 20 mL sample vial and 1 mL of decane was added. The mixture was heated with a heat gun until the solid dissolved, then the vial was left to cool to room temperature under ambient conditions (approx. 10 min). The sample vial was inverted and, if no flow was observed, it was deemed to be a gel. If the sample formed a gel, increments of 1 mL of decane were added to the vial and the heating-cooling process repeated until the gel flowed and did not pass the inversion test. The wt% was then calculated by using the largest volume of decane that was gelled by 5 mg of gelator (e.g. 5 mg of C_{12}-Ala-$CONH_2$ **2** can gel 7 mL of decane, which equals 0.10 wt%).

T_{gel} measurements

A metal heating block holding 4 mL vials (vial diameter = 15 mm) was heated from 70 to 125 °C in 5 °C increments. At each temperature, vials containing the gel sample were heated for 10 minutes. The vial was then removed and evaluated by the inversion test. The temperature at which the gel could no longer pass the inversion test was taken as the T_{gel} value. This process was done once from concentrations starting at 2 mg/mL to 10 mg/mL for both single and multicomponent systems.

UV-vis spectroscopy

Ultraviolet-visible (UV-vis) spectroscopy was performed on a Cary 5000 UV-Vis NIR spectrophotometer. Samples were prepared in 4 mL vials at a concentration of 5 mg/mL in decane. The gel in the vial was then heated until fully dissolved and transferred into a 10 mm pathlength glass cuvette where it was left to cool down and reform a gel. Each sample was analysed from 400 – 700 nm, using decane as a reference.

Rheology

Rheological properties of the gels were characterized at BC Research Inc. on a TA Instruments Discovery Hybrid Rheometer-2 using a 40 mm parallel plate. All measurements were conducted at 25 °C with an added layer of 400/P800 sandpaper on both plates to reduce gel slippage. All samples were prepared by dissolving 25 mg/mL of the gelator in decane, using a heat gun, and pouring the hot solution into a 10 cm diameter Petri dish. After 30 min, the gel was trimmed and transferred onto the rheometer plate. Frequency sweep experiments were performed from 0.1 to 100 rad/s at a strain% of 0.04 % to determine the viscoelastic moduli, the storage modulus G' and the loss modulus G" of the samples. All measurements were run in triplicate with a consistent gap of 1400 µm.

Scanning electron microscopy

Scanning electron microscopy (SEM) was performed at the UBC BioImaging Facility on a Hitachi S4700 electron microscope. Samples were prepared by placing a small quantity of the gelled sample (5 mg/mL) on an aluminium stub, which was left to air dry overnight. The samples were sputter-coated with an 8 nm coating of platinum/palladium alloy prior to imaging.

Differential scanning calorimetry

Thermal properties were characterized at BC Research Inc. on a TA Instruments DSC 250 differential scanning calorimeter using an aluminium pan. Wet gel samples in decane with a concentration of 20 mg/mL were deposited into the pan. They were heated from 40 to 155 °C at a rate of 10 °C/min. After remaining at the highest temperature for 0.5 min, the cooling run began at the same rate as heating. The temperature cycle was repeated 4 times, and the data from the last 3 cycles were used.

Single crystal X-ray diffraction

Single, colourless blade-shaped crystals of compound **3** were grown from a water/isopropanol (1:9) mixture by slow evaporation of the solvent. Single crystal X-ray diffraction (SCXRD) data were collected on a Bruker APEX-II CCD diffractometer at 100 K for **3** at the UBC X-ray Crystallography facility. Monochromated MoKα radiation (λ = 0.71 Å) was used and data were collected to a resolution of 0.93 Å. The structure was solved with the XT[26] structure solution program using the Intrinsic Phasing solution method and by using Olex2[27] as the graphical interface. The model was refined with version 2018/3 of XL using least squared minimisation[28]. All non-hydrogen atoms were refined anisotropically. Hydrogen atom positions were calculated geometrically and refined using the riding model; however, all N–H hydrogen atoms were located in difference maps and refined freely. A summary of the crystallographic data is reported for compound **1** in previous literature[23].

X-ray scattering

Wide angle X-ray scattering (WAXS) and small angle X-ray scattering (SAXS) were performed at 4D LABS at Simon Fraser University on a SAXSLAB Ganesha 300XL+. The samples had a concentration of 20 mg/mL for improved scattering. For the X-ray scattering, samples were prepared inside a Viton O-ring and sandwiched between two mica sheets (7 µm thick), enclosed within a stainless-steel disc. The samples were placed inside a vacuum chamber at $<5 \times 10^{-2}$ mbar pressure. The instrument uses CuKα radiation (1.5 Å) and the scattering pattern is measured by a Pilatus 300K 20 Hz X-ray detector (Dectris, Switzerland) positioned approximately 100 and 450 mm from the sample position for wide and small angles, respectively. All of the samples were measured at WAXS and SAXS configurations for 120 and 300 seconds, respectively. This was performed on individual gel samples and mixtures with 1:1 mass ratio.

Computer modelling

SAXS data were fit to a flexible cylinder model using SASView 4.0. Initial values were set as: Length = 10,000 Å, SLD = 9.4×10^{-6}, SLD_solvent = 7.2×10^{-6}. The polydispersity in radius was constrained to a value in the range 0.05 – 0.5. Observable peaks in the azimuthally regrouped SAXS data were fitted to a series of Pearson Type VII distributions using a non-linear Levenberg-Marquardt algorithm via the Imfit library in python. The peak positions and widths were extracted using this method to determine the d-spacing, d, and coherence length, D, defined as follows:

d-spacing $\boldsymbol{d = 2\pi/(peak\ centre)}$ (Eq 2.1)

Scherrer equation $\boldsymbol{D = b2\pi/(FWHM(Q))}$ (Eq 2.2)

where b is the Scherrer constant (0.9 for our sample[29]), FWHM refers to the full width at half maximum parameter in the Pearson type 7 distribution. It was not possible to determine values for d-spacing and coherence length for the **1+2** sample, due to lack of peaks.

The WAXS data were used to determine the internal structure for the samples in gel form, which could then be compared to the structure of the equivalent crystals, as observed in SCXRD. TOPAS 4.2 was used to model the data and compare unit cell parameters that were calculated from two different models. The first model used unit cell refinement where only the unit cell values were input with no atomic positions. The second model used a lattice parameter search where a dummy unit cell is input, and the fitting can occur unconstrained.

Results and discussion

The LMWGs (compounds **1**-**3**, Figure 3b) used in this study were prepared using a previously reported literature procedure[23] involving a substitution reaction between lauroyl chloride and amino acid amide. This class of LMWGs was previously studied for their ability to form gels in hydrophobic solvents such as decane, diesel and dilbit, with potential applications to oil spill remediation. The three LMWGs were based on phenylalaninamide, alaninamide and valinamide as they had the lowest minimum gelling concentrations; in this study, we investigated the effect of mixing these LMWGs to form multicomponent gels in decane, a solvent that was chosen as a mimic for hydrophobic oil slicks.

Gelation behaviour

Preliminary gelation studies were conducted using single components and multicomponent systems with equimass ratios to observe whether or not a gel was formed. The gelation abilities were evaluated using the gel-to-sol transition temperature (T_{gel}) and the inversion test[25], which requires no specialized equipment.

The minimum gelation concentrations (MGCs) of both single component gels and mixed component gels were determined (Table 1). A mixture of **1+3** has the lowest MGC (0.09 wt%), which is about the same as the single component gel of **1** (MGC = 0.1 wt%) and significantly lower than the gel formed from **3** alone (MGC = 0.3 wt%). The same effect was obtained for mixture **1+2**, where the multicomponent had an MGC (0.1 wt%) similar to that of **1**, but lower than the MGC of **2** (0.19 wt%). However, mixture **2+3** has an MGC of 0.21 wt%, which falls in between the MGCs of the single component gels of **2** and **3** (MGC = 0.19 and 0.3 wt%, respectively). This illustrates the unpredictable changes in gelation properties when transitioning between single component gels and multicomponent gels. To further understand the changes occurring upon mixing these LMWGs, we studied these systems using SEM, DSC and X-ray scattering.

Table 1. Minimum gelling concentrations (MGCs) for individual and multicomponent gels in decane (n=3).

Sample	MGC (wt%)	Error (±wt%)
1	0.10	0.031
2	0.19	0.076
3	0.30	0.064
1+2	0.10	0.014
1+3	0.09	0.0072
2+3	0.21	0.035

The thermal stability of a gel is often characterized using gel-to-sol phase boundary transition temperatures (T_{gel})[22]. We determined the T_{gel} values by heating the gels from 70 to 125 °C in 5 °C increments until the gel no longer passed the inversion test. As expected, a general trend of increasing T_{gel} with increasing concentration was observed (Figure S1). The gel network becomes thermally more stable with increased concentration due to the presence of additional molecular interactions, which results in a higher T_{gel}.

Table 2. UV-Vis transmittance at 650 nm for single and multicomponent gels (varying mass ratios).

Sample	Ratio	Transmittance (%) at 650 nm*
1		2.3
2		4.0
3		0.38
1+2	1:4	75
	1:2	84
	1:1	89
	2:1	90
	4:1	78
1+3	1:4	7.5
	1:2	27
	1:1	70
	2:1	95
	4:1	96
2+3	1:4	0.31
	1:2	9.9
	1:1	80
	2:1	82
	4:1	74

*error estimate of 0.1%

Optical properties

As illustrated in Figure 3, the mixtures of LMWGs show different optical properties from their constituent LMWGs. In particular, the transparency of the mixed component gel systems could be tuned by varying the mass ratio of the LMWGs. This phenomenon was studied using ultraviolet-visible (UV-vis) spectroscopy, allowing the transparency to be determined through %transmittance across the spectrum. Table 2 shows the %transmittance at the chosen wavelength of 650 nm for single component gels and the mixtures with varying mass ratios, while Figure 4 shows the complete UV-vis spectra of all the mass ratios for the single and multicomponent gels. Figure 4a highlights the drastic difference in transmission between the single component LMWGs and equimass mixtures of pairs of LMWGs **1**-**3** (mixed in 1:1 wt. ratio). The transmittance is very low for the single component systems, consistent with the gel's opaqueness, while the higher transmittance for the mixtures was consistent with the more transparent nature of the gel as observed with the naked eye. Table 2 shows how the transmittance is influenced by changing the ratio of the components. As the ratio for component **1** increases in mixtures of **1+2**, the transmittance is found to have a bell curve, where percentage transmittance increases until a maximum (90 %T for **1+2** at 2:1 ratio), and then decreases when component **1** is in greater excess. A similar trend was found for **2+3**: as the proportion of **2** increased, the transmittance rises until a maximum and then decreases. For mixtures of **1+3** we see a rising transmittance as the

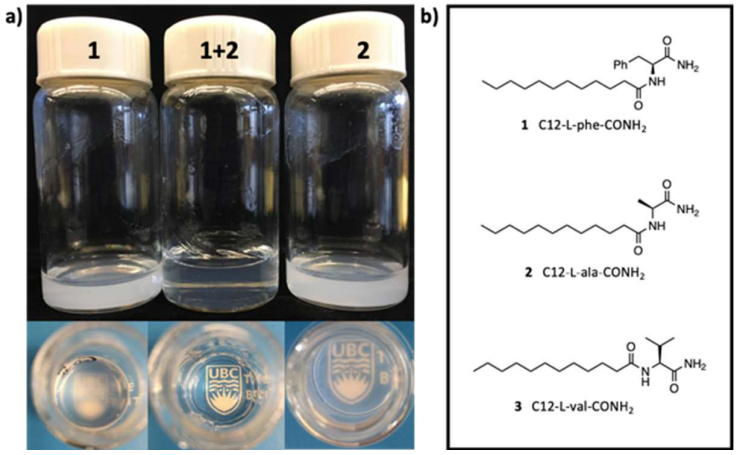

Fig. 3 a) Photographs showing the appearance of gels made from single gelators and a multicomponent system (1:1 mass ratio) from a side and top view showing the difference in opacity, and b) Chemical structures of LMWGs **1**-**3** explored in this study.

quantity of **1** increases, with a high of 96 %T at weight ratio 4:1. These trends represent the dependence each individual component has on the other in terms of the gel's optical properties. For mixtures **1+2** and **2+3**, there is an optimal ratio, which is 2:1 for both mixtures, that yields the gel with maximum transmission at 650 nm. Mixture **1+3** has a maximum transmission at a ratio of 4:1, though higher proportions of **1** were not explored.

The enhanced transparency of the mixed gel systems suggests that incident light undergoes less scattering as it passes through the gel. Since Rayleigh scattering depends on the size of the particles ($\propto d^6$ for spherical particles), we believe that the particles are larger in the single component LMWGs than in the mixed component LMWGs. Indeed, SEM observations of the gel support this (*vide supra*). Thus, mixtures of LMWGs can yield smaller fibres, reducing the amount of scattering from the particles. This could be due to changes in solubility, packing arrangement, or hydrophobic interactions.

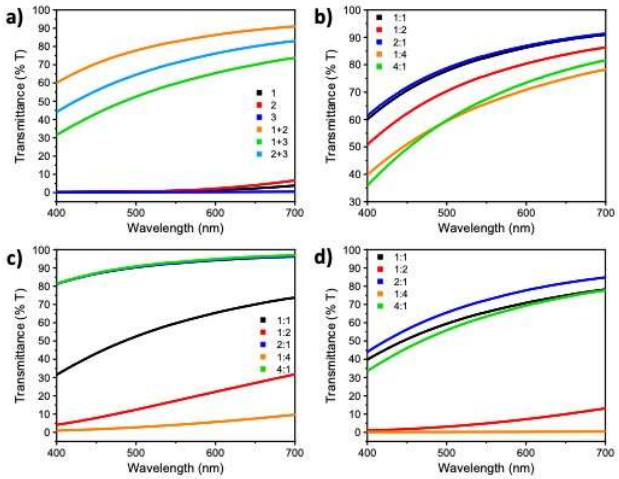

Fig. 4 UV-vis spectra of gels with a concentration of 5 mg/mL a) of individual and multicomponent at 1:1 equimass ratio. b) **1+2** mixture with varying ratios. c) **1+3** mixture of varying ratios. d) **2+3** mixture of varying ratios.

To analyse the UV-vis spectra in Figure 4, where transmittance increases with increasing wavelength, the data were transformed into the graphs plotted in Figures 5 and S2. Remarkably, when the data were transformed to plot 1/(%Absorbance) versus wavelength (λ), the curves fit perfectly to a quadratic function. This indicates that the curvature observed in the plots shown in Figure 4 is not due to Rayleigh scattering, as it would have a $1/\lambda^4$ dependence instead of a $1/\lambda^2$ dependence. We hypothesize that the inverse-square dependence could be due to circular birefringence, as the molecules are chiral[30], or due to index of refraction, however this work is still ongoing.

Mechanical properties

The mechanical properties of the bulk gel were characterized using a rheometer. The response to changes in frequency at a constant strain was investigated for single and multicomponent gel systems. Figure 6 depicts the average complex modulus from three frequency sweeps for both individual and mixed (1:1 ratio) systems to compare the stiffness of the gels. This is indeed observed for mixtures **1+2** and **1+3**, where the complex modulus is situated between the values for the individual components. For mixture **2+3**, however, the complex modulus is significantly higher than that of either individual component, indicating that the mixture is stiffer than both of its constituents. From the complex modulus of these gel systems, we observe different behaviours in stiffness of the materials, where mixtures yield a stiffer material, seen for **2+3**, or an average of each individual component, seen in **1+2** and **1+3**. This again highlights the difficulties faced when attempting to determine the properties of multicomponent gel systems.

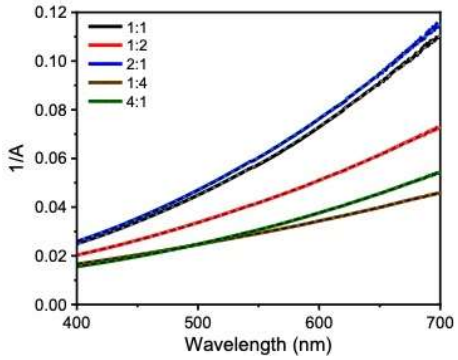

Fig. 5 UV-vis spectra from the **1+2** mixture plotted as the inverse of the absorbance vs the wavelength. Experimental data is represented by the solid lines and the corresponding fits to quadratic functions are shown by the dashed lines.

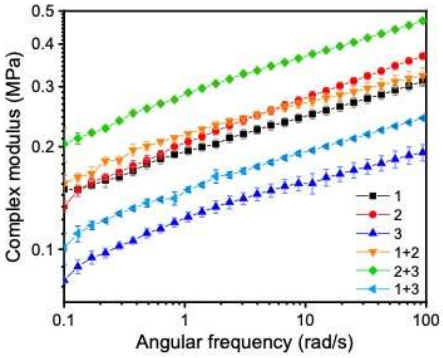

Fig. 6 Frequency sweep of single and multicomponent gels (1:1 ratio) in decane, showing the average complex modulus of three runs at a strain of 0.04%. Error bars represent one standard deviation (n = 3).

Packing of gelators

Multicomponent gelator systems in which each individual component is capable of forming a gel have two main ways of packing as a mixture: co-assembly and self-sorting (Figure 2). In co-assembly, the two molecules interact with each other to yield fibres with both components in the interconnected gel network. In self-sorting, the molecules interact preferentially with molecules of the same type, and therefore assemble independently to form two distinct structures but interpenetrating within a gel network. In a multicomponent gel network, it is possible for the assembly of two gelators to occur in between the two extremes of co-assembly and self-sorting to varying degrees[7].

To distinguish between the two assembly methods in a multicomponent system, various characterization techniques are required to probe all length scales in order to understand the nature of the packing within the gel. Different techniques are used to determine molecular interactions, fibre structure / dimensions, interconnected network and bulk gel properties, all of which represent different properties of the gel[21]. In determining the difference and dominance between co-assembly and self-sorting, the interconnected network was probed through scanning electron microscopy (SEM) as this technique shows the morphology of the gel network, where the xerogel of a mixture can be compared to the individual components for fibre characteristics and cluster formations. Investigating the bulk gel uses differential scanning calorimetry (DSC) for thermostability information, in terms of physical transformations within the gel when it is heated and cooled over multiple cycles. This gives details on how the gel disintegrates and assembles, and can be compared to the behaviour of the single components. To observe and quantify structural features at the nano- and Angstrom-scales, small and wide-angle scattering techniques are required. The scattering of each gel's fibre will differ, however certain characteristics in the scattering pattern will convey information about the fibre packing, specifically in mixtures compared to individual gels. These three techniques probe different length scales of the gel to determine whether co-assembly or self-sorting is more dominant for a certain multicomponent gel system. We employed these techniques to resolve the packing nature of our mixed gel systems.

Morphology

Scanning electron microscopy (SEM) was used to investigate the morphology of the gels in the form of xerogels. Samples were prepared using equimass ratio for mixtures and the pure individual gels at a concentration of 5 mg/mL. This collapsed system of the xerogel can give a good indication of fibre characteristics and rough fibre sizes for comparison.

The SEM images, Figure 7, show that the fibre characteristics of each individual gelator, **1**, **2**, and **3**, are different. Pure **1** contains long intertwined fibres with some alignment, whereas pure **2** is comprised of coiled fibres with no specific orientation. Pure **3** presents plate-like rigid fibres. The pure single component systems display thicker diameter fibres, possibly accounting for their opaque nature, and consistent with the decreased transmittance observed by UV-vis spectroscopy (Figure 4a). Opaque gels have microscale structures that scatter more light, whereas transparent gels exhibit nanoscale features[22], which are observed in the mixed gel systems. Qualitatively, the fibres of the multicomponent gels appear thinner with a narrower distribution of radii in comparison to individual gels, therefore contributing to the transparency. The mixed gel systems do not have a well-defined configuration but instead a more integrated system where the two components are indistinguishable via electron microscopy images. With respect to packing, SEM suggests co-assembly rather than self-sorting of the components as the xerogel shows characteristics of both components with no clusters or aggregation. In a self-sorted system, one would expect a clear divide with clusters, due to the incompatibility of the two molecules[31].

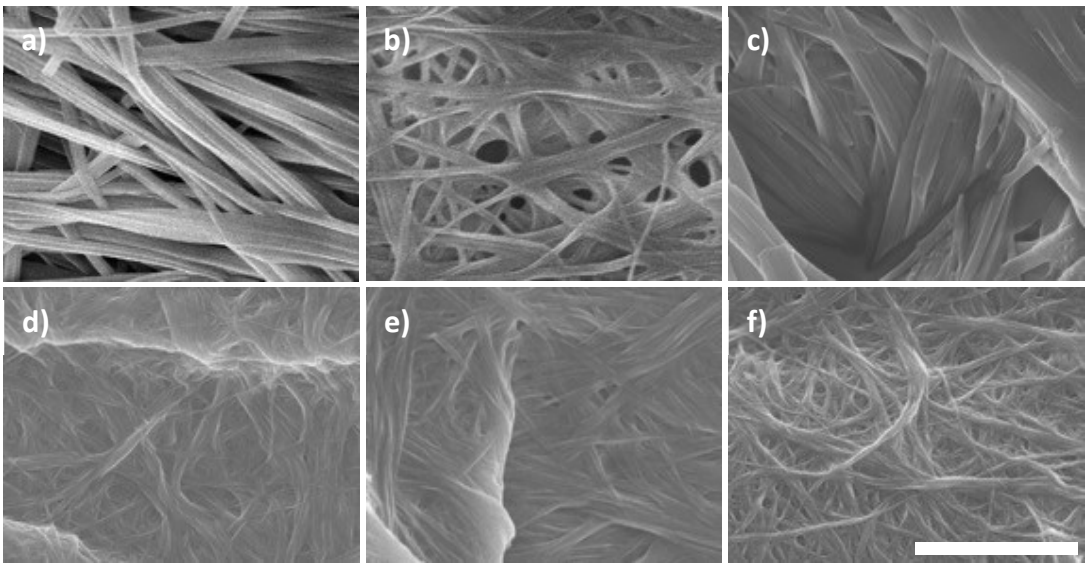

Fig. 7 SEM images of xerogels from a concentration of 5 mg/mL in decane. Images of compounds a) **1**, b) **2**, c) **3**, d) **1+2**, e) **1+3**, f) **2+3**. Scale bar = 2 μm.

Thermostability

DSC of multicomponent systems can give insight into a gel's packing motif as the endothermic gel-sol transition represents the disintegration of the 3D network. Figure 8a shows the DSC trace of the average heating and cooling cycle of gel mixture **1+2** and the individual components, **1** and **2**. The endothermic gel-sol transition temperature for **1** is 92.0 °C, while for **2** it is 129.0 °C. In comparison, the gel-sol transition temperature for the equimass mixture of **1+2** is at 111.4 °C, which falls between the individual components. The same effect is seen in the sol-gel transition where the temperatures for **1** and **2** (75.2 and 112.8 °C, respectively) sandwich the transition temperature of the multicomponent gel of **1+2** (81.5 °C). The fact that only one transition is observed in each mixture (not separate peaks corresponding to each component, as sometimes observed in self-sorted systems[32]) and that they lie in between the individual components supports a co-assembly model for the gelators.

We also analysed the mixed systems **1+3** and **2+3** by DSC (Figure S3). They also showed single transition peaks that did not match either individual component. Thus, DSC further provides evidence of co-assembly in the multicomponent systems.

X-ray scattering

To further distinguish between co-assembly and self-sorting, small angle X-ray scattering (SAXS) was performed to probe the internal structure of the gels at the nanoscale. Figure 8b shows the SAXS data for mixture **1+2** and the individual components, showing the difference in scattering between all three compositions. Compound **1** has a sharp peak at q ≈ 0.28 $Å^{-1}$, while compound **2** has a peak at q ≈ 0.2 $Å^{-1}$, reflecting the difference in packing between the different compounds. Multicomponent equimass gel **1+2**, however, lacks any distinct peaks. Furthermore, the resulting SAXS data were fit to a flexible cylinder model using SASView 4.0 (Figure 9 & S5). This allowed the fibre radius, d-spacing and coherence length to be determined for each gel system. The radii of single component gels were found to be approximately 68 Å, 119 Å, and 169 Å for compounds **1**, **2** and **3**, respectively. The radii of the multicomponent gels were both much smaller and closer in magnitude to each other; approximately 40 Å, 43 Å to 48 Å for mixtures **1+2**, **1+3**, and **2+3**, respectively. From the resulting estimations, the single component gels have a higher fibre radius than multicomponent gels. This agrees with SEM observations (Figure 7), where thinner fibres are seen in mixed systems, which contributes to the transparency observed in the bulk (Figure 3a)[33].

The peaks in the scattering patterns were used to calculate the d-spacing and coherence length of the gel systems. The lack of peaks in mixture **1+2** made it challenging to determine values for d-spacing and coherence length; therefore, no data are shown. The d-spacing values can be compared to single crystal X-ray diffraction (SCXRD) of the molecules to compare molecular packing within the gel to the packing in the crystal. Crystals for SCXRD were grown in 1:9 water and isopropanol for compounds **1**[23] and **3** (Figure S6a,b), while SAXS was performed on gels swelled in decane. (Despite many attempts, we could not grow single crystals of compound **2**). When comparing the d-spacing calculated for the main peak from the SAXS data with the unit cell dimensions of SCXRD (Figure S6c,d) we find reasonable agreement between the crystallographic c axis value and the d-spacing. For compound **1**, the calculated d-spacing is 23.3 Å and c value is 23.17 Å, while for compound **3**, the d-spacing is 31.0 Å and c value is 30.36 Å. This agreement indicates that the molecular packing between the gel and solid-state samples is similar when taking into account that the d-spacing value is slightly larger than the c value due to the presence of solvent molecules in the gels. When comparing the d-spacing of the individual compounds with mixture **1+3**, we find that the value is approximately halfway between that of **1** and **3** at 26.6 Å. This trend is not true for mixture **2+3**, where **2** = 31.5 Å, **3** = 31.0 Å and **2+3** = 34.7 Å, which may be due to a difference in the compatibility of the compounds when forming a mixture. Additionally, the predicted powder diffraction pattern, as obtained from the SCXRD data, was compared to WAXS data, where no

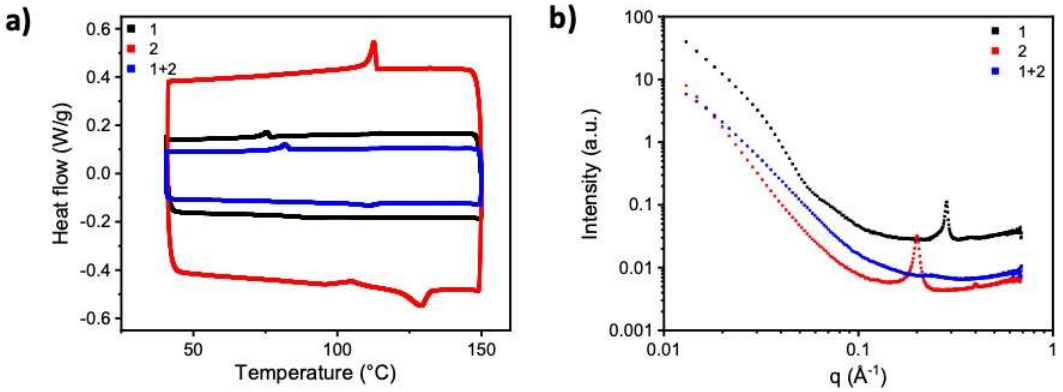

Fig. 8 DSC trace showing the average heating and cooling cycle of mixture 1+2 and the respective individual compounds 1 and 2. b) SAXS data for 1 alone, 2 alone, and 1+2 mixture.

preferred fibre orientation was observed, for compounds **1** and **3** (Figure S7 & S8). The resulting unit cell parameters modelled (Table S1) showed good agreement for **3** with the SCXRD unit cell indicating with confidence that the molecules in the gel are organized in a similar manner to those in the crystal state. For compound **1**, the modelled unit cell parameters were similar, however with lower confidence.

In Figure 8b, a slight broad peak is observed between the peaks of **1** and **2**, but it cannot be associated with either compound. A general trend observed in mixed gel systems from X-ray scattering is the broadening or disappearance of peaks, which indicates loss of crystallinity within the system from a single component system. In a self-sorted system, similar to DSC, one would expect the mixture to have characteristics of both individual compounds with peaks present at the same q value. However, this is not observed and, instead, the mixtures show fibre morphologies and peaks that are not observed in either of their constituent components, an indication of co-assembly occurring in the mixed systems.

The calculated coherence lengths (Table 3) from peak width, allows us to quantify the long-range order present in the nanostructure. From Figure 8b & S4 it can be observed from the SAXS data that individual gels have at least one sharp peak present, while

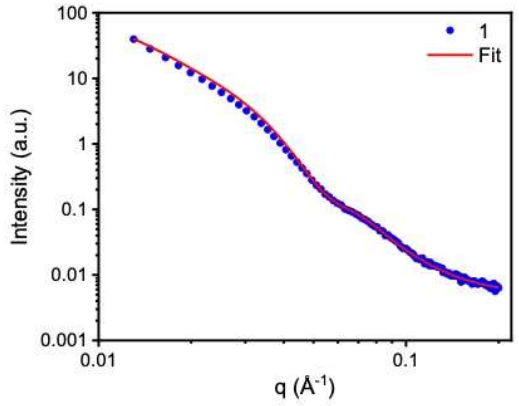

Fig. 9 Plot of radially averaged intensity vs. q for SAXS data taken from compound 1 at a concentration of 20 mg/ml. The solid line represents the fit to a flexible cylinder model.

mixed gels have either broader peaks or no peaks at all, as in the case of **1+2**. The coherence lengths are therefore shorter in mixed gel systems, indicating a decrease in long-range order upon mixing.

Table 3. Summary of the fit parameters for all measured samples.

Sample	Radius (Å)	d-spacing (Å)	Coherence length (Å)
1	68.4 ±0.03	22.1	151
2	119.1 ±0.77	31.5	460
3	169.0 ±0.23	31.0	270
1+2	39.6 ±0.07	-	-
1+3	43.2 ±0.04	26.4	274
2+3	47.5 ±0.04	34.7	104

An analysis of the X-ray scattering data supports the hypothesis that the transparency seen in the macroscopic state is due to thinner fibres in the multicomponent systems. With this we also observe a loss of crystallinity and long-range order in comparison to single component gels. In terms of packing, specifically for single-component gels, the packing of molecules in the crystalline state translate into the gel state, seen through d-spacing and PXRD data fitting. Furthermore, SAXS data are consistent with DSC and SEM that co-assembly packing is favoured in our multicomponent gel systems rather than self-sorting.

Conclusions

We investigated the effect of mixing three amino acid-based LMWGs on the gel properties in comparison to their single component gel systems. Mixing two LMWGs resulted in gels that showed enhanced optical and mechanical properties, measured through UV-Vis spectroscopy and rheology. We found that the transparency of the gels could be tuned by changing the mass ratio of each gelator in multicomponent gels, enabling access to gels that range from opaque to translucent to highly transparent in the same solvent. This unique phenomenon allows tunability without introducing another variable into the system, making it a desirable concept for optical applications. To further study the nature of the

multicomponent gels, they were investigated by SEM, DSC and SAXS. Together, the results of these techniques indicate that the gels form through co-assembly rather than self-sorting. This suggests that the interactions between the headgroups are similar, and the slight variations still facilitate co-assembly. Analysis of the SAXS data allowed us to determine fibre radii and coherence lengths of single and multicomponent gels, as well as compare with SCXRD data. We found that the general molecular packing in the crystal structure of two of the LMWGs is indeed translated into the gel phase. This allowed us to correlate SCXRD with SAXS data, which aids in understanding the packing preferences of a gel. As shown, mixed gel systems are more complicated and unpredictable than single component gels but allow access to new material properties in gels that are inaccessible in single component systems.

Conflicts of interest

There are no conflicts to declare.

Acknowledgements

We thank NSERC (Discovery Grant to MJM), MITACs (internship to JNL), and BC Research Inc. for funding this research. We thank Prof. Mark Thachuk for useful discussions to understand the optical properties of the mixtures. We thank Dr. Brian Patrick and Anita Lam for the collection and interpretation of SCXRD data.

Notes and references

1 N. Annabi, A. Tamayol, J. A. Uquillas, M. Akbari, L. E. Bertassoni, C. Cha, G. Camci-unal, M. R. Dokmeci, N. A. Peppas and A. Khademhosseini, *Adv. Mater.*, 2014, 85–124.

2 B. N. A. Peppas, J. Z. Hilt, A. Khademhosseini and R. Langer, *Adv. Mater.*, 2006, **18**, 1345–1360.

3 A. K. Gaharwar, N. A. Peppas and A. Khademhosseini, *Biotechnol. Bioeng.*, 2014, **111**, 441–453.

4 S. Kawano, N. Fujita and S. Shinkai, *Chem. A Eur. J.*, 2005, **11**, 4735–4742.

5 S. Yagai, S. Kubota, T. Iwashima, K. Kishikawa, T. Nakanishi, T. Karatsu and A. Kitamura, *Chem. - Eur. J.*, 2008, **14**, 5246–5257.

6 T. Kitamura, S. Nakaso, N. Mizoshita, Y. Tochigi, T. Shimomura, M. Moriyama, K. Ito and T. Kato, *J. Am. Chem. Soc.*, 2005, **127**, 14769–14775.

7 L. E. Buerkle and S. J. Rowan, *Chem. Soc. Rev.*, 2012, **14**, 6089–6102.

8 D. M. Ryan, B. L. Nilsson, D. M. Ryan and B. L. Nilsson, *Polym. Chem.*, 2012, **3**, 18–33.

9 M. C. Branco and J. P. Schneider, *Acta Biomater.*, 2009, **5**, 817–831.

10 D. Bardelang, M. B. Zaman, I. L. Moudrakovski, S. Pawsey, J. C. Margeson, D. Wang, X. Wu, J. A. Ripmeester, C. I. Ratcliffe and K. Yu, *Adv. Mater.*, 2008, **20**, 4517–4520.

11 S. Yagai, T. Nakajima, K. Kishikawa, S. Kohmoto, T. Karatsu and A. Kitamura, *J. Am. Chem. Soc.*, 2005, **127**, 11134–11139.

12 P. Mukhopadhyay, Y. Iwashita, M. Shirakawa, S. Kawano, N. Fujita and S. Shinkai, *Angew. Chem., Int. Ed.*, 2006, **45**, 1592–1595.

13 S. S. Babu, V. K. Praveen and A. Ajayaghosh, *Chem. Rev.*, 2014, **114**, 1973–2129.

14 J. D. Tovar, *Acc. Chem. Res.*, 2013, **46**, 1527–1537.

15 B. Escuder, B. Escuder, F. Rodrı and J. F. Miravet, *New J. Chem.*, 2010, **34**, 1044–1054.

16 C. Berdugo, B. Escuder and J. F. Miravet, *Org. Biomol. Chem.*, 2015, **13**, 592–600.

17 D. Diaz, D. Kühbeck and R. J. Koopmans, *Chem. Soc. Rev.*, 2011, **40**, 427–448.

18 J. J. D. De Jong, L. N. Lucas, R. M. Kellogg, J. H. van Esch and B. L. Feringa, *Science*, 2004, **304**, 278–282.

19 S. Bhuniya and B. H. Kim, *Chem. Commun.*, 2006, 1842–1844.

20 D.-C. Lee, K. K. Mcgrath and K. Jang, *Chem. Commun.*, 2008, 3636–3638.

21 E. R. Draper and D. J. Adams, *Chem*, 2017, **3**, 390–410.

22 D. K. Smith, in *Organic Nanostructures*, 2008, pp. 111–154.

23 J. Chen, C. E. Boott, L. Lewis, A. Siu, R. Al-Debasi, V. Carta, A. A. Fogh, D. Z. Kurek, L. Wang, M. J. Maclachlan and G. Hum, *ACS Omega*, 2020, in press.

24 J. Raeburn, D. J. Adams and D. J. Adams, *Chem. Commun.*, 2015, **51**, 5170–5180.

25 R. G. Weiss and P. Terech, Eds., *Molecular Gels: Materials with Self-Assembled Fibrillar Networks*, Springer, 2006.

26 G. M. Sheldrick, *Acta Crystallogr.*, 2014, **A71**, 3–8.

27 O. V Dolomanov, L. J. Bourhis, R. J. Gildea, J. A. K. Howard and H. Puschmann, *J. Appl. Crystallogr.*, 2009, **42**, 339–341.

28 G. M. Sheldrick, *Acta Crystallogr.*, 2014, **C71**, 3–8.

29 H. P. Klung and L. E. Alexander, *X-ray diffraction procedure for polycrystalline and amorphous materials*, 1974.

30 L. Poladian, M. Straton, A. Docherty and A. Argyros, *Opt. Express*, 2011, **19**, 968–980.

31 J. R. Moffat and D. K. Smith, *Chem. Commun.*, 2009, 316–318.

32 M. M. Smith and D. K. Smith, *Soft Matter*, 2011, **7**, 4856–4860.

33 G. Feng, H. Chen, J. Cai, J. Wen and X. Liu, *Soft Mater.*, 2014, 403.